01,05

Features of the phase composition and structure of hypoeutectoid steel, manifested in the behavior of magnetization near magnetic saturation

© S.V. Komogortsev, S.V. Semenov, S.N. Varnakov, D.A. Balaev¶

Kirensky Institute of Physics, Federal Research Center KSC SB, Russian Academy of Sciences, Krasnoyarsk, Russia

¶ E-mail: dabalaev@iph.krasn.ru

Received August 28, 2021
Revised August 28, 2021
Accepted September 3, 2021

Investigation of the temperature evolution of magnetization curves near magnetic saturation makes it possible to extract new information on the features of the phase composition and structure of hypoeutectoid steel. It is shown that the main contribution to the magnitude and the temperature behavior of the energy density of the local magnetic anisotropy of hypoeutectoid steel is due to the lamellar structure of pearlite. The peculiarity of the temperature behavior of the energy of the magnetic anisotropy, along with the behavior of the paraprocess, indicates the formation of Mn-substituted cementite in the studied steel sample. The observation of the crossover of power-law regularities in the approximation of magnetization to saturation indicates the formation of two-dimensional nano-inhomogeneities of the local axis of easy magnetization in the plates of alpha iron, which are part of the pearlite.

Keywords: magnetization, steel, cementite, iron, approach to saturation magnetization, pearlite

DOI: 10.21883/PSS.2022.01.52484.192

1. Introduction

Steel is one of the leaders among the materials that are in demand in practice, that's why the study of its structure and properties is closely entwined into the history of humankind, science and technology. Following the main paradigm of the material science, steel structure at different scales (from the scale of interatomic distances to tens of microns) and its relation to properties have been studied in great detail and are being still studied (adequate citation here seems simply impossible, that's why we will refer to two of the latest monographs dealing with the history and current state of the issue [1,2]). New information, as in any „hot" field of the material science, appears here in relation to the progress of measuring equipment that allows for using previously unavailable (due to various reasons) approaches and methods for analysis of the structure or properties. It can be exemplified by the progress in the use of microscopical methods that allow for finding new things in the steel structure on the nanoscale [3,4].

Magnetic structural methods hold a prominent place in steel studies and interesting opportunities here appear in relation to wide spreading of new high-accuracy magnetometric equipment that allows for operational carrying-out of studies in high fields and a wide temperature range. The well-known method of magnetic phase analysis [5] in this respect may provide new opportunities upon obtaining of information not only about the phase composition, but also about the peculiarities of micro- and nanostructure [6,7]. According to the conventional magnetic phase analysis, based on temperature dependence of magnetization $M(T)$, it is possible both to identify a phase according to Curie temperature value (e.g., for classical cementite Fe_3C $T_C = 480\,K$) and to assess its amount by presenting $M(T)$ as a sum of partial contributions to magnetization by individual phases [5]. It is interesting to take information about perlite, a permanent structural component of steel, from magnetic measurements. Perlite is a product of eutectoid decomposition of austenite under relatively slow cooling of iron carbon alloys below 727°C [1,2] and is a mixture of two phases: BCC-Fe, containing from 0.006 to 0.025% of carbon and cementite. Lamellar perlite, where both phases alternate and have the lamella shape, is the main perlite kind within hypoeutectoid steels. Our paper demonstrates how the perlite lamellar structure manifests itself in results of magnetometric measurements and, thus, how information provided by such measurements can be used for studying this important structural component of hypoeutectoid steel. Moreover, this paper demonstrates the additional possibilities of hypoeutectoid steel study by using modern magnetometric equipment and development of approaches to processing of the data near magnetic saturation.

It should be also noted that development of methods for analysis of structural steels' magnetic properties is related to one more task: the need to understand the processes taking place in steels operating in corrosive environments at high temperatures, e.g., as elements of electrolytic baths in aluminum production. In this case, the behavior of magnetization of the electrolytic bath material is important for monitoring and simulation of magnetohydrodynamic parameters of electrolyser operation [8,9].

2. Experiment

A specimen of structural steel St-3 was studied (GOST 380-2005) [10]. Samples for measurements were made in the shape of a ball weighing about 80 mg (sample temperature during sample preparation did not rise above 120°C).

Magnetic measurements (curves of magnetization $M(H)$ and temperature dependences of magnetization $M(T)$) were performed using a LakeShore VSM 8604 vibration magnetometer. Dependences of $M(H)$ and $M(T)$ were measured at temperature rise. Since irreversible transformations took place at temperatures above 1000 K, the sample was heated only once, and then a new sample of the initial steel was measured. The sample was demagnetized prior to each measurement of $M(H)$. Dependences of $M(H)$ (magnetic field strength) were adjusted with account of the sample shape factor [11].

3. Results and discussion

3.1. Temperature behavior of magnetization in a field of 10 kOe

Temperature trend of magnetization, measured in the field $H = 10$ kOe (Fig. 1, *a*), reflects both the magnetic subsystem's peculiarities (Curie temperature for BCC-iron $T_C \approx 1043$ K) and structural transformations in steel at high temperatures (near the temperature of steel eutectoid transformation at $T_e \approx 1000$ K [1,2]). The specified temperatures T_C and T_e manifest themselves distinctly on the dM/dT derivative shown in Fig. 1, *b*.

Hypoeutectoid steel with the carbon content of $0.14 \div 0.22$ wt.% contains from 2.2 to 3.4 wt.% of cementite. Cementite transition to a paramagnetic state above 480 K (Curie temperature for classical cementite) [5,12] shall cause a step on the temperature trend of magnetization near this temperature, however, such a step within the available measurement accuracy is not reliably observed. Taking into account the fact that cementite is characterized by a high constant of magnetocrystalline anisotropy and the fact that the perlite microstructure can generate a high magnetostatic local magnetic anisotropy, it can be supposed that the field of 10 kOe is insufficient for full technical saturation. Then, these doubts can be solved by analyzing the curves of magnetization approach to saturation in different temperatures.

3.2. Magnetization approach to saturation

Figure 2 gives the curves of magnetization $M(H)$ in the temperature range of $80 \div 1200$ K in (H, T, M) coordinates. It should be noted that the dependences of $M(H)$ in rather large fields have a tendency towards attainment of saturation (a permanent value of magnetization). Thereat,

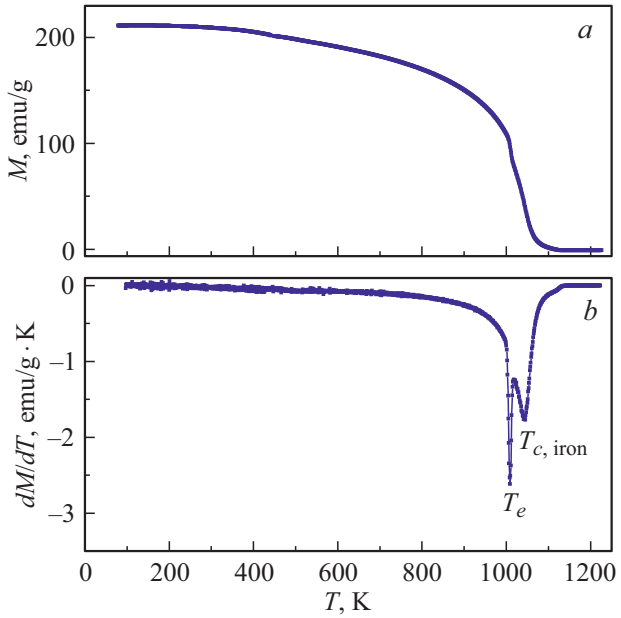

Figure 1. Temperature dependence $M(T)$ — (*a*) in the field $H = 10$ kOe and its derivative dM/dT — (*b*) for the studied steel sample.

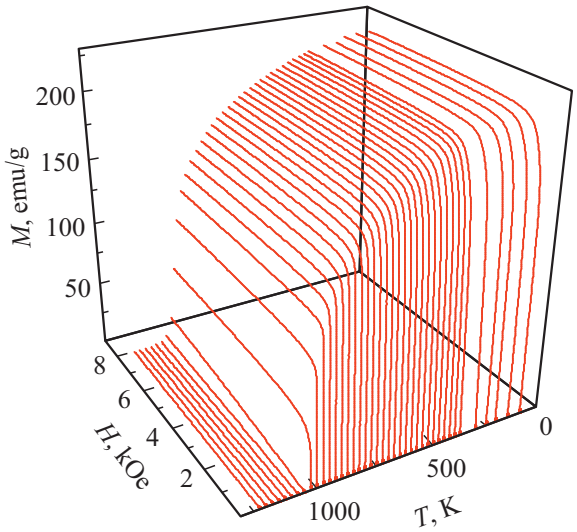

Figure 2. Steel magnetization curves measured at different temperatures.

the following dependence is observed

$$M(H) = M_s \cdot (1 - A \cdot H^{-2}), \qquad (1)$$

known as the N.S. Akulov law of attainment of saturation (in the expression (1) A is a constant). This is illustrated in Fig. 3, where selective representative dependences of $M(H)$ are given in (H^{-2}, M) coordinates. Correspondence of the data to the straight lines in Fig. 3 means fulfillment of the dependence (1). The selective data of Fig. 3 show that the field range of fulfillment of the dependence (1) decreases as temperature increases. The Akulov law describes the

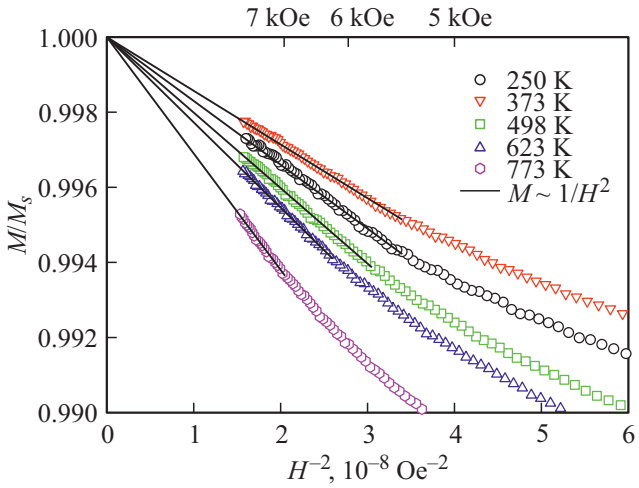

Figure 3. Preliminary analysis of magnetization approach to saturation in (H^{-2}, M) coordinates for estimating the sufficiency of the equation (1) in experiment description.

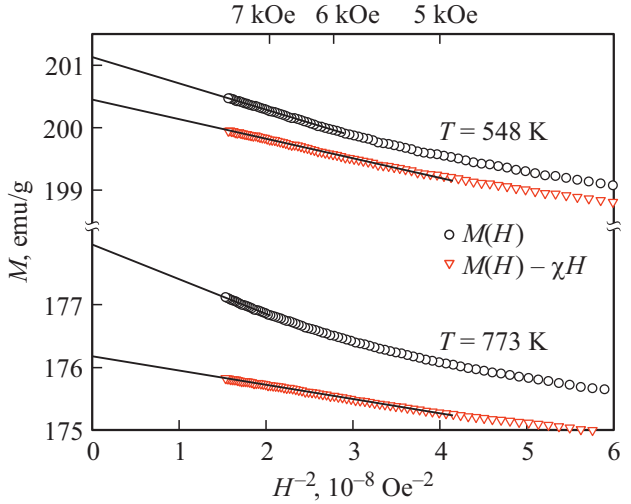

Figure 4. Effect of consideration of the paraprocess contribution for description magnetization approach to saturation.

approach to saturation of a ferromagnetic substance with a randomly oriented axis of easy magnetization of local magnetic anisotropy [13–15] and reflects the competition of local magnetic anisotropy, related to various discontinuities of the structure and external field.

Based on the „Occam's razor" principle, the use of the equation (1) may seem sufficient for describing the curves of magnetization in high fields. However, our attempts at such a description show that the range of fields where this dependence is fulfilled is shortened upon temperature rise, while the coefficient A increases. This makes us doubtful of correctness and sufficiency of the use of the equation (1) only. In reality, one more summand, related to magnetic susceptibility, must be taken into account for magnetization approach to saturation in ferromagnetic materials, iron in particular: the so-called paraprocess $\chi \cdot H$, induced in the magnetic subsystem of a ferromagnetic substance as a result of competition of high fields and thermal fluctuations [16,17]. Approach to saturation in this case should be described by a more complex equation

$$M(H) = M_s \cdot (1 - A \cdot H^{-2}) + \chi \cdot H. \qquad (2)$$

Figure 4 shows that consideration of the summand $\chi \cdot H$ enlarges the field region where the magnetization curve straightens in (H^{-2}, M) coordinates. Moreover, such a description leads to a physically reasonable decrease of the coefficient A as temperature rises (Fig. 7). An intermediate conclusion, resulting from such data handling: magnetization approach to saturation of the studied steel in the range of 5 to 8 kOe is well described by the expression (2). Figure 2, which contains all the magnetization curves, shows an increased role of the second summand upon a transition through the Curie temperature for BCC-iron, which is confirmed quantitatively by a preliminary description of the data by the equation (2).

Taking into consideration the aforesaid, computer fitting of the measured curve of $M(H)$ by the dependence (2) was carried out in the field range of 5 to 8 kOe. This range also meets the condition: value of the first nonlinear summand in the equation (2) does not exceed 1% of the composite signal. A check of smallness of the summands in the equation (2) is related to the fact that the theoretical expressions, subsequently used for data analysis, have been obtained on the assumption of small deviations of magnetization on full saturation. Quality of fitting to the temperature of 975 K is rather satisfactory; deviations of fitting curves from the experimental data are homogeneous and agree with the values of random error of magnetization measurements (Fig. 5). The parameter A above 1043 K was so small that only the second summand was used during fitting by the equation (2).

3.3. Temperature evolution of the parameters that characterize the magnetization approach to saturation and their relation to microstructural peculiarities of steel

The values of fitting parameters (M_s, A, χ), obtained as a result of fitting of magnetization approach to saturation from 5 to 8 kOe, allow for tracing changes in the magnetic subsystem of steel as temperature changes. Quantity M_s is a result of extrapolation of the technical saturation process to infinite fields and can be considered as a quantity of spontaneous magnetization at the given temperature. Figure 6 compares the data on M_s with the predictions of the formula

$$M_s = M_{s0} \cdot \left[1 - s \cdot (T/T_c)^{3/2} - (1 - s) \cdot (T/T_c)^p\right]^{1/3}, \quad (3)$$

recently suggested in the paper [18] as a universal formula for a wide class of ferromagnetic materials. This formula assumes that the low-temperature behavior of magnetization follows the so-called Bloch law $T^{3/2}$ applicability of which

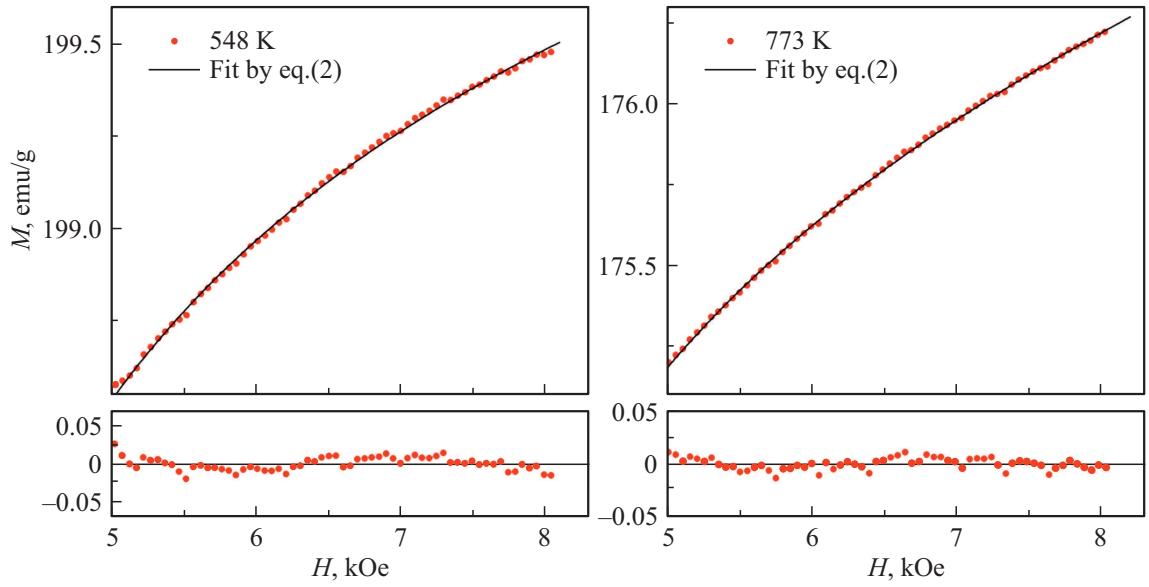

Figure 5. Fitting of the measured magnetization curve (symbols) by the equation (2). The lower inserts show a deviation of the measured magnetization on predictions of the equation (2).

for metals and metal alloys was discussed earlier and is still being discussed lately [7,19–23]. A point of accord in these discussions, however, is the fact that such behavior must be described by a power law of the $M \propto T^n$ type, the argument deals only with the value of the power exponent ($n = 3/2$ or 2). Since the minimum temperature at which we measured the magnetization curve was 85 K, it can be stated that the „disputable" low-temperature area is outside the range of the obtained data. On the whole, as seen from Fig. 6, there is a remarkable agreement between the data and predictions of the formula (3) during selection of the fitting parameters given in the legend to Fig. 6. The main weight fraction of the material ($\approx 97\%$) is BCC-iron. This, apparently, manifests itself in the fact that the value of the parameter $p = 4$ coincides with the one for pure Fe, being insignificantly different from the values for other ferromagnetic substances [18]. The parameter $s = 0.57$ slightly differs from the parameter for pure iron ($s = 0.35$) given in [18]. Some deviations above 975 K are probably due to a partially completed eutectoid transformation in steel (see par. 3.1 and Fig. 1).

Temperature behavior of high-field magnetic susceptibility (Fig. 7), in addition to the peculiarity related to Curie temperature of BCC-Fe, reveals a small peak between 205 and 250 K. Curie temperature of Fe_3C, however, is much higher (about 480 K) [24]. The arguments that the observed peak reflects the Curie temperature of Mn-substituted cementite in the studied steel sample are given below.

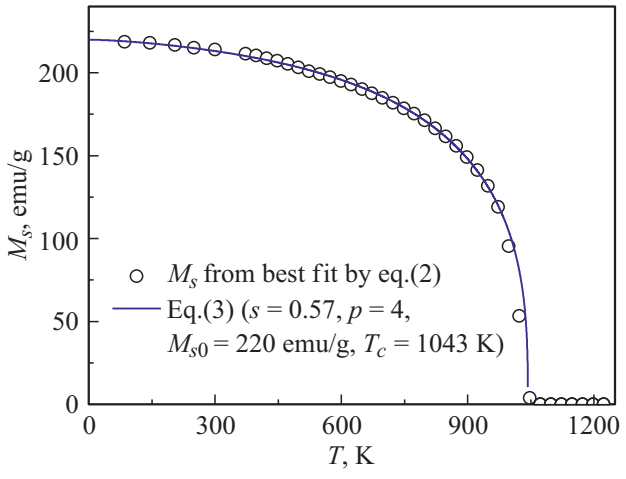

Figure 6. Temperature behavior of steel saturation magnetization and its description by equation (3).

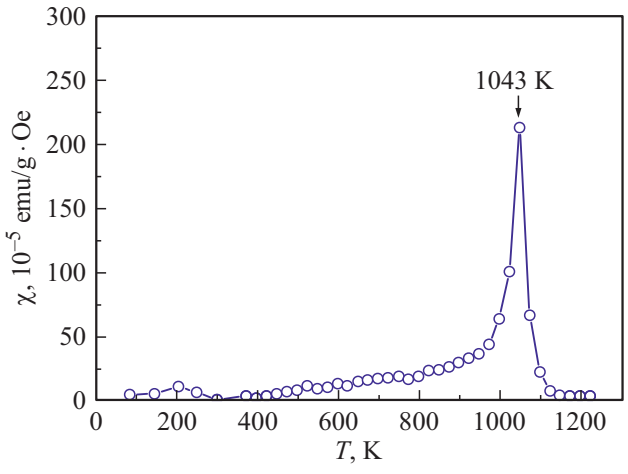

Figure 7. Temperature behavior of high-field magnetic susceptibility of steel.

The coefficient A in the expression (2) is a total result of various contributions that cause inhomogeneity of magnetization in a finite field, and can be considered as a particular measure for energy density of local magnetic anisotropy. Temperature behavior of the coefficient A is shown in Fig. 8. If the value of A is estimated only as a contribution by magnetocrystalline anisotropy of alpha iron as $A = \frac{2}{105} H_{a,\mathrm{Fe}}^2$ (the red dot-and-dash line in Fig. 8), it turns out that the measured values of A by more than an order exceed this estimate (estimation used the known data for BCC-Fe [17,25]). Thus, the other contributions, including the cementite contribution, cannot be neglected in this case, considering that the main material fraction (97 wt.%) falls on alpha iron. Then we will analyze the dependence $A(T)$ as a sum of the following contributions [13,26–30], considered as the essential ones at the next stage in clarification of our behavior analysis of $A(T)$:

$$A = \frac{2}{105} H_{a,\mathrm{Fe}}^2 (1-x) + \frac{1}{15} H_{a,\mathrm{Fe_3C}}^2 \cdot x + \frac{1}{15} \left[4\pi (M_{s,\mathrm{Fe}} - M_{s,\mathrm{Fe_3C}}) \cdot p(1-p)\right]^2 \cdot y, \quad (4)$$

here, x is the cementite fraction in steel, y is the pearlite fraction in steel ($y = 0.26$ is adopted for the given steel sample), p is the cementite fraction in pearlite, $H_{a,\mathrm{Fe}}$, $H_{a,\mathrm{Fe_3C}}$ are fields of magnetocrystalline anisotropy for alpha iron and cementite, $M_{s,\mathrm{Fe}}$, $M_{s,\mathrm{Fe_3C}}$ are saturation magnetizations for alpha iron and cementite. The first and second summands in the expression (4) give the contributions by magnetocrystalline anisotropy of randomly oriented alpha iron and cementite crystallites. The difference in numerical coefficients in case of these summands reflects the difference in the phase symmetry of alpha iron (cubic 2/105) and cementite (uniaxial 1/15) [14]. The third summand takes into account the magnetic anisotropy caused by inhomogeneous pearlite structure (shown schematically on the right in Fig. 9). The build of this summand reflects the idea that the pearlite lamellar structure (Fig. 9) must cause inhomogeneity of the magnetic static field, which will generate a local magnetic anisotropy induced by the magnetic anisotropy of the lamella shape, difference of their magnetizations and their volume ratios.

For quantitative comparison of the experimental dependence of $A(T)$ with the expression (4) we have used the published anisotropy constants of BCC-Fe [17,25] and cementite [31,32], as well as the Akulov–Zener law that establishes the temperature behavior of ferromagnetic substance anisotropy constants and agrees well with the experiment [17,33]:

$$K(T) = K(0) \cdot \left(M_s(T)/M_s(0)\right)^m. \quad (5)$$

The anisotropy fields that make part of the equation (4) are related to the anisotropy constants as $H_a = 2 \cdot K/M_s$. The indicator is $m = 10$ for BCC-Fe (cubic anisotropy)

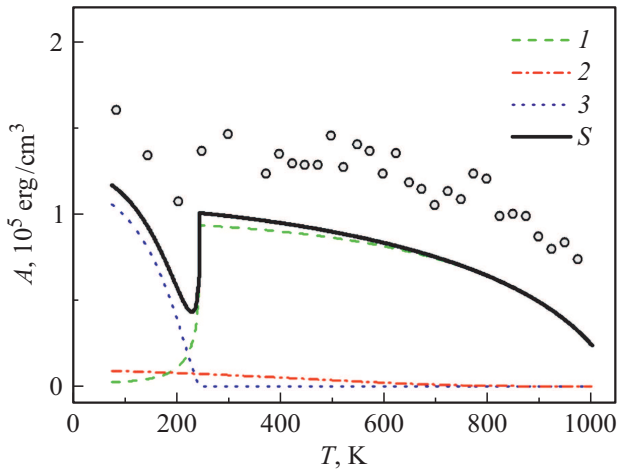

Figure 8. Temperature behavior of the coefficient A, obtained by data fitting by the equation (2) (symbols) and estimated using the equation (4) (the thick black line — total estimate, thin colored lines — contributions of various summands in the equation (4): *1* — magnetostatic contribution of pearlite; *2* — contribution of magnetocrystalline anisotropy of BCC-Fe; *3* — contribution of cementite magnetocrystalline anisotropy).

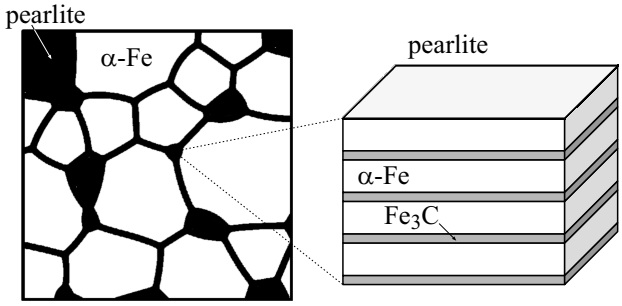

Figure 9. Schematic view of the microstructure of hypoeutectoid steel — on the right, pearlite structure — on the left.

and $m = 3$ for cementite (uniaxial anisotropy) [14]. The behavior of $M_s(T)$ for alpha iron and cementite was estimated according to the equation (3), using the parameters of $M_s(0)$ from [17,25,31,32], for alpha iron we adopted $T_C = 1043$ K, for cementite we chose $T_C^* = 240$ K (this choice is justified below), the other parameters in the equation (3) were taken equal to the alpha iron parameters [18].

It can be seen from Fig. 8 that the total behavior of the contributions (expression (4)) describes the experimental data with accuracy up to a certain permanent contribution. Figure 7 also shows that, in the temperatures that exceed the temperature transition of cementite to the paramagnetic state, the main contribution to the temperature behavior of $A(T)$ is by the magnetostatic contribution of the pearlite structure. Moreover, a transition across the cementite Curie temperature inevitably leads to a stepwise change in the contribution related to magnetostatic anisotropy of pearlite,

due to an abrupt change in interaction between the lamellas of BCC-iron in the pearlite structure. The peculiarity related to T_C of cementite is in the range of 200−250 K, i.e. in the same place where the magnetic susceptibility peak is observed, see Fig. 7. Such an abrupt decrease of cementite T_C as compared to the known Curie temperature of Fe_3C (480 K) may be caused by partial substitution of iron atoms by manganese atoms. Manganese in the studied hypoeutectoid steel (St-3) is a mandatory component ($0.4 \div 0.65$ wt.%). Negative enthalpy of formation of Mn_3C (−20 kJ/mole) [34] in modulus is significantly higher than the maximum enthalpy of formation of BCC Fe-Mn solid solutions (−1 kJ/mole) [35]. It means that upon pearlite formation in steel St-3, when homogeneous austenite must break down into cementite and BCC-Fe, it is more preferable (from the energy viewpoint) for the manganese atoms (initially distributed uniformly in the austenite) to become a part of cementite. Taking into account the Mn content in the studied sample, the composition of Mn-substituted cementite $(Mn_xFe_{1-x})_3C$ can be expected to vary within $x = 0.11 \div 0.185$. According to the data of the papers [36,37], which studied the magnetic properties of Mn-substituted cementite, Curie temperatures at such a substitution level must be observed in the range of 140 to 280 K. Since the cementite Curie temperature of $200 \div 250$ K, observed in Figs. 7 and 8, is within this range, we may conclude that Mn-substituted cementite forms in the studied steel sample. This conclusion looks unexpected given the fact that manganese addition in commercial-quality steels is justified by the need for deoxidation (removal of residual oxygen) [10,38]. The obtained result means that sometimes, as apparently happened in our case, manganese addition, given the small amount of residual oxygen, instead of the anticipated deoxidation, embeds into cementite, thereby changing its properties (Curie temperature).

A constant-value difference between the data of $A(T)$, obtained experimentally, and the expression (4) (see Fig. 8), can be related to the contributions not taken into account in the equation (4). In the first place, this is a magnetoelastic contribution, related to the presence of internal stresses in steel [26,27], then, a contribution to the constant of local magnetic anisotropy by the so-called surface magnetic anisotropy [39,40] can be expected in pearlite characterized by a well-developed phase contact area and, finally, the magnetocrystalline anisotropy constant for Mn-substituted cementite can be higher than the anisotropy constant of Fe_3C used for assessment by means of the equation (4). Correct consideration of these contributions requires additional experimental research. At this stage, we confine ourselves to stating the good qualitative agreement between the data and estimate in Fig. 8, which allows for drawing the following conclusions: 1) the observed peculiarity (minimum) near $T_C^* \sim 240$ K on $A(T)$ reflects the Curie temperature of Mn-substituted cementite; 2) the main contribution to the value and temperature behavior of $A(T)$ above T_C^* is related to the pearlite lamellar structure. These findings also mean that the used approaches are a useful tool to analysis of pearlite state in hypoeutectoid steel.

3.4. Crossover of power regularity of magnetization approach to saturation

In order to trace the power regimes in the magnetization approach to saturation, the value of $(M_s - (M(H) - \chi \cdot H))/M_s$ (so-called magnetization dispersion [41–43]), according to the equation (2), that gives a non-linear contribution into the magnetization approach to saturation, is given in Fig. 10 depending on the external field in double logarithmic coordinates. A deviation from full technical saturation, for the data of Fig. 10, plotted on the ordinate axis, does not exceed 2%, thus, the main provisions of the theory of magnetization approach to saturation hold good. The area described by a non-linear summand from the equation (2) for various $M(H)$ is observed here as a straight line with an inclination tangent of −2. It can be also seen that the power behavior (straight lines with inclination tangents of −0.75 to −1) is observed below 4 kOe for different temperatures (covering almost the whole studied temperature range).

Power exponents in the range of $-0.75 \div -1$, according to the papers [41–44], correspond to two-dimensional correlations of magnetization. As shown in par. 3.3, the main contribution to deviation of magnetization from saturation is made by the pearlite structure. In this case, it is natural to expect that the observed two-dimensional pattern of magnetization correlations will also be related to the lamellar structure of pearlite, which facilitates the propagation of correlations in the plane, but hinders such propagation across the plane of pearlite lamellas. The size of structural inhomogeneities (correlation length of the local axis of easy magnetization) can be estimated from the value of the field $H_R \approx 4.5$ kOe of a change in the power dependences; this field is observed in Fig. 10 as $l_c = \sqrt{2C/(M_s H_R)}$ [43], where $C = 2.1 \cdot 10^{-6}$ erg/cm is

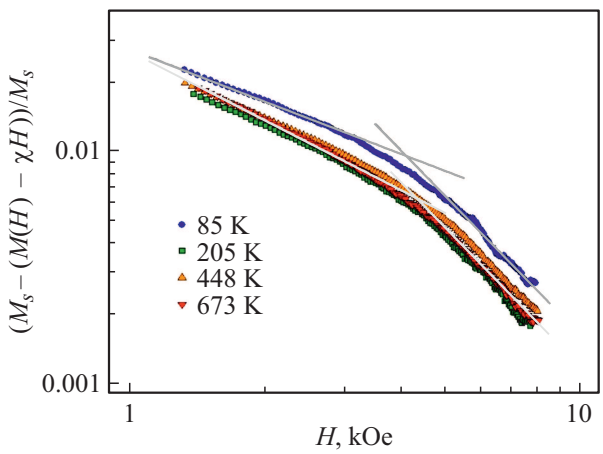

Figure 10. Power regularities manifesting themselves in the field behavior of magnetization deviation from saturation (straight-line portions).

the exchange interaction constant for alpha iron [20]. Estimation gives $l_c \approx 8$ nm. Such a small size means that the iron within pearlite lamellas is structurally inhomogeneous on the nanoscale. According to the papers [45,46], in combination with the observed manifestations of the two-dimensional pattern of magnetization correlations, this also means the so-called anisomery of structural inhomogeneities of alpha iron within pearlite lamellas. The term „anisomeric inhomogeneities" means that the region of homogeneous orientation of a local axis of easy magnetization is localized in two dimensions on significantly shorter scales than in the third one [44]. It can be naturally expected for alpha iron lamellas in pearlite that two such dimensions are in the lamella plane, while the third one is perpendicular to it (the above-mentioned estimate $l_c \approx 8$ nm apparently refers to the size of the inhomogeneity in the lamella plane).

4. Conclusion

The study of temperature and field behavior of magnetization of a hypoeutectoid steel sample St-3 near the magnetic saturation by means of modern magnetometric equipment, allows for obtaining new information both about the magnetic subsystem's behavior and about the peculiarities of the phase composition and structure of hypoeutectoid steel (in particular, about the state of pearlite in hypoeutectoid steel). Let us summarize the main observations and conclusions of the paper to illustrate this.

The temperature dependence of magnetization in rather a large external field ($H = 10$ kOe) has peculiarities related both to irreversible transformations (in the vicinity of temperature of steel eutectoid transformation $T_e \approx 1000$ K) and to reversible transformation ferromagnetic–paramagnetic at T_C (≈ 1043 K).

Magnetization curves for hypoeutectoid steel in the region of approach to magnetic saturation are successfully described by means of the Akulov law taking into account the paraprocess-related summand, which is characterized by magnetic susceptibility χ. The latter summand makes a large contribution to magnetization near the Curie temperature, while magnetic susceptibility demonstrates a peak at T_C (≈ 1043 K). In the vicinity of $200 \div 250$ K there is one more peak on the dependence $\chi(T)$. Based on the analysis of magnetization approach to saturation, we relate this peak (near $T_C^* \sim 240$ K) to the Curie temperature of substituted cementite $(Fe, Mn)_3C$ that forms in the pearlite structure of hypoeutectoid steel. It has been showed that the temperature trend of steel saturation magnetization is successfully described by the universal equation suggested in the paper [18]. The magnetostatic inhomogeneity, related to the pearlite lamellar structure, makes the main contribution to the energy value of local magnetic anisotropy, which leads to a slower, as compared to pure iron, approach of magnetization to technical saturation. In the vicinity of the cementite Curie temperature there is a stepwise change in the energy of local magnetic anisotropy, related to an abrupt change in exchange and dipole-dipole interactions between iron and cementite lamellas in the pearlite structure. Observation of a change in power regularities in magnetization approach to saturation means the formation of two-dimensional nanoirregularities of the local axis of easy magnetization in alpha iron lamellas included in the pearlite.

Finally, we would like to note that the conclusions concerning the structure and phase composition, made on the basis of magnetostructural studies shall be subsequently verified using direct methods of structure and phase composition study.

Funding

The research has been conducted with financial support by the Russian Foundation for Basic Research, Government of the Krasnoyarsk Territory, Krasnoyarsk Regional Science Foundation within the framework of the scientific project No. 20-48-242905 p_Yenisei Siberia „Determining the impact of ferromagnetic magnetization on MHD parameters of electrolyser operation".

The magnetic measurements have been performed using the equipment of the Shared-Access Equipment Center of Federal Research Center „Krasnoyarsk Science Center of the Siberian Branch of the Russian Academy of Sciences".

Conflict of interest

The authors declare that they have no conflict of interest.

References

[1] W. Pepperhoff, M. Acet. Constitution and Magnetism of Iron and its Alloys. Springer Berlin Heidelberg, Berlin, Heidelberg (2001). 213 p.
[2] H. Bhadeshia, R. Honeycombe. Iron-Carbon Equilibrium and Plain Carbon Steels. In: Steels Microstruct. Prop. Elsevier (2017). P. 59–100.
[3] Y. Li, D. Raabe, M. Herbig, P.-P. Choi, S. Goto, A. Kostka, H. Yarita, C. Borchers, R. Kirchheim. Phys. Rev. Lett. **113**, 106104 (2014).
[4] M. Reibold, P. Paufler, A.A. Levin, W. Kochmann, N. Pätzke, D.C. Meyer. Nature **444**, 286 (2006).
[5] B.A. Apaev. Fazovyi magnitnyi analiz splavov. Metallurgiya, M. (1976). 283 p.
[6] L.A. Chekanova, E.A. Denisova, O.A. Goncharova, S.V. Komogortsev, R.S. Iskhakov. Physics of Metals and Metallography **114**, 136 (2013).
[7] S.N. Varnakov, J. Bartolome, J. Sesé, S.G. Ovchinnikov, S.V. Komogortsev, A.S. Parshin, G.V. Bondarenko. Physics of the Solid State **49**, 1401 (2007).
[8] M. Dupuis, V. Bojarevics, J. Freibergs. Light Metals TMS (The Minerals, Metals & Materials Society). 453 (2004).
[9] V. Bojarevics, E. Radionov, Y. Tretiyakov. Light Metals / Ed. O. Martin. The Minerals, Metals & Materials Series. 551–556 (2018). DOI: 10.1007/978-3-319-72284-9_72

[10] Stal uglerodistaya obyknovennogo kachestva (GOST 380-2005), RF(2008) (in Russian).
[11] S. Chikazumi. Physics of Ferromagnetism. 2nd ed. (2009). 672 p.
[12] S.W.J. Smith, W. White, S.G. Barker. Proc. Phys. Soc. London. **24**, 62 (1911).
[13] N.S. Akulov. Zeitschrift Phys. **69**, 822 (1931).
[14] V.A. Ignatchenko, R.S. Iskhakov, G.V. Popov. JETP **82**, 1518–1531 (1982).
[15] R.S. Iskhakov, S.V. Komogortsev. Phys. Met. Metallogr. **112**, 666 (2011).
[16] K.P. Belov. Physics-Uspekhi **65**, 207 (1958).
[17] S.V. Vonsovskiy. Magnetism. Nauka. M. (1971). 1032 p. (in Russian).
[18] M.D. Kuz'min. Phys. Rev. Lett. **94**, 107204 (2005).
[19] B.P. Khrustalev, A.D. Balaev, V.G. Pozdnyakov. Thin Solid Films **130**, 195 (1985).
[20] R.S. Iskhakov, S.V. Komogortsev, A.D. Balayev, A.V. Okotrub, A.G. Kudashov, V.L. Kuznetsov, Yu.V. Butenko. JETP Letters **78**, 271 (2003).
[21] N.B. Melnikov, B.I. Rezer. Theoretical and Mathematical Physics **181**, 358 (2014).
[22] D.A. Balaev, S.V. Semenov, S.N. Varnakov, E.Y. Radionov, Y.A. Tretyakov. J. Sib. Fed. Univ. Math. Phys. **14**, 5 (2021).
[23] U.Köbler. J. Magn. Magn. Mater. **491**, 165632 (2019).
[24] H.K.D.H. Bhadeshia. Int. Mater. Rev. **65**, 1 (2020).
[25] L.V. Kirenskiy, V.P. Ryabinin. Kristallografiya **7**, 644 (1962) (in Russian).
[26] N.S. Akulov, L.V. Kirenskiy. Technical Physics **9**, 1145 (1939).
[27] L.V. Kirenskiy, L.I. Slobodskoy. Dokl. AN SSSR **70**, 809–811 (1950) (in Russian).
[28] H. Kronmuüller, A. Seeger. J. Phys. Chem. Solids **18**, 93 (1961).
[29] V.V. Parfenov, Yu.P. Lobastov. PMM **16**, 334 (1963).
[30] M. Fähnle, H. Kronmüller. J. Magn. Magn. Mater. **8**, 149 (1978).
[31] S. Yamamoto, T. Terai, T. Fukuda, K. Sato, T. Kakeshita, S. Horii, M. Ito, M. Yonemura. J. Magn. Magn. Mater. **451**, 1 (2018).
[32] S.V. Komogortsev, R.S. Iskhakov, A.D. Balayev, A.G. Kudashov, A.V. Okotrub, S.I. Smirnov. Physics of the Solid State **49**, 700 (2007).
[33] C. Zener. Phys. Rev. **96**, 1335 (1954).
[34] J. Briki, S. Ben Slima. J. Met. **2012**, 1 (2012).
[35] V.T. Witusiewicz, F. Sommer, E.J. Mittemeijer. Met. Mater. Trans. B **34**, 209 (2003).
[36] G.P. Huffman, P.R. Errington, R.M. Fisher. Phys. Status Solidi **22**, 473 (1967).
[37] A.I. Ulyanov, A.A. Chulkina, V.A. Volkov, E.P. Elsukov, A.V. Zagaynov, A.V. Protasov, I.A. Zykina. Physics of Metals and Metallography **113**, 1201 (2012).
[38] B.N. Arzamasov, I.I. Sidorin, G.F. Kosolapov. Materialovedeniye. Mashinostoenie, M. (1986). 384 p. (in Russian).
[39] D.A. Balaev, I.S. Poperechny, A.A. Krasikov, K.A. Shaikhutdinov, A.A. Dubrovskiy, S.I. Popkov, A.D. Balaev, S.S. Yakushkin, G.A. Bukhtiyarova, O.N. Martyanov, Y.L. Raikher. J. Appl. Phys. **117**, 063908 (2015).
[40] D.A. Balaev, I.S. Poperechny, A.A. Krasikov, S.V. Semenov, S.I. Popkov, Y.V. Knyazev, V.L. Kirillov, S.S. Yakushkin, O.N. Martyanov, Y.L. Raikher. J. Phys. D **54**, 275003 (2021).
[41] H. Hoffmann. J. Appl. Phys. **35**, 1790 (1964).
[42] K.J. Harte. J. Appl. Phys. **39**, 1503 (1968).
[43] R.S. Iskhakov, V.A. Ignatchenko, S.V. Komogortsev, A.D. Balayev. JETP Letters **78**, 1142 (2003).
[44] V.A. Ignatchenko. JETP **54**, 303 (1968).
[45] V.A. Ignatchenko, R.S. Iskhakov. Physics of Metals and Metallography **6**, 75 (1992).
[46] R.S. Iskhakov, S.V. Komogortsev, A.D. Balaev, A.A. Gavriliuk. J. Magn. Magn. Mater. **374**, 423 (2015).